

Turrietta, E. and Reidenbach M.A., 2024, Edge effects of a fragmented seagrass habitat on flow, bivalve recruitment, and sediment dynamics, *Marine Ecology Progress Series*, 732, 52-71
<http://doi.org/10.3354/meps14545>

1 **Edge effects of a fragmented seagrass habitat on flow, bivalve recruitment, and sediment**
2 **dynamics**

5 Elise Turrietta¹ and Matthew A. Reidenbach^{1*}

8 ¹Department of Environmental Sciences, University of Virginia, Charlottesville, Virginia 22904,
9 USA

12 *Corresponding Author: Matthew Reidenbach (mar5jj@virginia.edu)

14 **Running page head: Fragmented Seagrass Hydrodynamics**

16 **Abstract**

17 In both continuous and fragmented seagrass ecosystems, the vegetation edge can be a
18 location of abrupt hydrodynamic change, with impacts to both ecological and physical processes.
19 We address how flow and wave activity change across seagrass meadow edges and the effects of
20 vegetation on sediment dynamics and bivalve recruitment. Two *Zostera marina* seagrass
21 meadow sites were monitored, a high-density site with > 500 shoots m^{-2} and a low-density site
22 with < 250 shoots m^{-2} . Mean flow velocities were significantly reduced in seagrass vegetation
23 adjacent to edges, with reductions compared to unvegetated areas ranging from 30% to 75%.
24 Recruitment of juvenile bivalves was significantly elevated within vegetation. No significant
25 differences in wave activity or sediment suspension/deposition were found spatially across a 10
26 m distance from a seagrass edge, but significant temporal variability was observed caused by
27 periodic storms. Wave height was a major predictor for sediment movement along seagrass
28 edges, with an observed tenfold increase in sediment collection within benthic traps following
29 severe storms. These results were found across various heterogeneous edge configurations and
30 reveal abrupt hydrodynamic responses of both mean flow and turbulence to occur at short spatial
31 scales (1 to 10 m), with changes to wave and sediment deposition/suspension conditions only
32 occurring over larger spatial distances (~ 100 m). Changes to the hydrodynamic regime were
33 therefore found to be driven on daily timescales by meteorological conditions (e. g., winds,
34 storms) and on longer temporal and/or spatial timescales by changes in seagrass shoot density,
35 altering both bivalve recruitment and sediment dynamics.

36 **Keywords:** Seagrass, hydrodynamics, bivalve larvae, sediment resuspension, fragmentation,
37 recruitment

39 1. INTRODUCTION

40 Seagrass meadows provide an extensive range of ecosystem services, including coastal
41 protection, faunal habitats, carbon sequestration, and enhanced water quality (Aoki et al. 2020,
42 Oreska et al. 2020). However, as human development and use of coastal landscapes increase
43 along with a warming climate (Allen et al. 2021), seagrass ecosystems have been degraded
44 globally (Dunic et al. 2021). This degradation has spurred restoration efforts and has
45 simultaneously generated questions regarding how alterations of these vegetated environments
46 lead to ecological and physical consequences and state changes (McGlathery et al. 2013).
47 Seagrasses also have extensive influence on hydrodynamic patterns by inducing drag on the
48 surrounding flow. This leads to velocity gradients and the formation of boundary layers at
49 several spatial scales, from turbulence generation around individual blades to reduced flow
50 across an entire meadow (Koch et al. 2006, Nepf 2012, Reidenbach & Thomas 2018).

51

52 1.1 Flow conditions in seagrass

53 Within the canopy, Hansen & Reidenbach (2012) found seagrass presence to reduce near-
54 bottom mean velocities by up to 90% compared to unvegetated regions. The induced drag also
55 alters velocity profiles, as a shear layer forms at the interface of the canopy and overlying water
56 (Gambi et al. 1990), creating regions of increased velocity above the top of the canopy and
57 reduced flow below it (Ghisalberti & Nepf 2002). At high seagrass densities, ‘skimming flow’
58 can occur, where increased velocity above the canopy arises as the amount of bulk water flow
59 through the canopy is substantially reduced (Koch & Gust 1999, Hansen & Reidenbach 2017).
60 Seagrass density and patch morphology also influence turbulence regimes, with high blade

61 densities (> 500 shoots m^{-2}) resulting in a stronger turbulent shear layer above the canopy and
62 reduced mixing below it (Nepf & Vivoni 2000, Hansen & Reidenbach 2012). However, at low
63 densities (< 200 shoots m^{-2}), flow can penetrate within the canopy and increase turbulence
64 caused by stem-wake interactions (Fonseca & Koehl 2006, Hansen & Reidenbach 2013).

65 It has been well established that seagrass presence also results in wave attenuation
66 (Twomey et al. 2020). However, the degree of attenuation depends on whether the prevailing
67 flow conditions are driven by winds or tidally-driven currents (Zhu et al. 2021) and the
68 characteristics of the waves influence the extent of seagrass response (Bradley & Houser 2009).
69 Results from both modeling and experimental studies have shown that higher seagrass density
70 and biomass leads to greater attenuation in wave height, but depends upon the spatial extent of
71 the meadow (Chen et al. 2007, Bradley & Houser 2009), with Reidenbach & Thomas (2018)
72 showing attenuation of wave heights across hundreds of meters of meadow. At the smaller patch
73 scale, El Allaoui et al. (2016) found that more fragmented canopies resulted in less attenuation of
74 waves and increased mean flow velocities, and that fragmented seagrass environments are less
75 efficient at providing a sheltering habitat against high flow conditions. Theoretical, laboratory
76 and field studies have also shown that substantial reductions of in-canopy velocities are expected
77 for mean flows or for low frequency waves when the orbital excursions are larger than the
78 canopy drag length scale, which is a function of seagrass blade geometry and spacing (Lowe et
79 al. 2005; 2007, Luhar et al. 2010). However, little is known about how changes to flow
80 conditions along a fragmented seagrass landscape occur that might impact sediment and larval
81 settlement dynamics on both short term (wave-driven storm conditions) and longer term (spring-
82 neap tidal cycles) hydrodynamic forcings.

84 1.2 Hydrodynamic impacts on sediment suspension and deposition

85 Generally, oscillatory motions caused by waves penetrate deeper into the seagrass canopy
86 than tidally driven flow, and can interact with the seafloor to create a velocity gradient at the
87 sediment-water interface (Koch & Gust 1999, Hansen & Reidenbach 2012). The presence of
88 waves, when combined with current flow, results in a separate, combined wave-current boundary
89 layer (Grant & Madsen 1979) which enhances bottom shear stresses that can exceed the critical
90 stress threshold necessary for sediment resuspension (Reidenbach & Timmerman 2019). The
91 strength of the bed shear formed at the sediment-water interface often determines local
92 suspended sediment concentrations (SSCs) (Lawson et al. 2007), while tidal currents largely
93 control the net sediment transport through the system at large (Jing & Ridd 1996). The presence
94 of seagrass alters the magnitude of these flow-sediment interactions (Donatelli et al. 2018, Zhu et
95 al. 2022). Hansen & Reidenbach (2012) found that in a combined wave-current flow, bed shear
96 stress in bare areas often exceeded the critical stress threshold to initiate sediment movement, but
97 at vegetated sites the bed shear stress was lower than this critical value 80% of the time. The
98 reduction in sediment resuspension within seagrass ecosystems can be attributed to the reduction
99 of canopy flow velocity as well sediment stabilization by the seagrass roots (Gacia & Duarte
100 2001, Nardin et al. 2018).

101 Because of this limited resuspension, seagrass meadows are often considered depositional
102 environments for sediment which may create a positive feedback loop where more light
103 availability encourages more seagrass growth, further reducing SSCs (Adams et al. 2016).
104 Recent work by Zhu et al. (2021) modeled the effects of flow-wave-vegetation interaction at a
105 meadow scale and concluded that vegetation density mediated the response of SSCs and
106 sediment transport. Seasonally, higher-density vegetation in the summer (> 200 shoots/m²)

107 significantly attenuated flow, waves, and SSCs, but lower-density vegetation (< 160 shoots/m²)
108 in the winter resulted in much smaller SSC reductions. Under similar conditions, meadow edges
109 were the most sensitive to changes in erosional or depositional conditions and controlled the
110 amount of suspended sediment advected throughout the system at large (Zhu et al. 2022).

111

112 1.3 Bivalve settlement, recruitment, and abundance

113 In addition to their pronounced effect on flow regimes, seagrass presence has been linked
114 to increased species richness, diversity, density, and abundance of associated macrofauna (Orth
115 et al. 1984, Bologna & Heck 2002). Studies have shown significant positive correlations between
116 bivalve abundance and seagrass density and biomass (Peterson et al. 1984, Glaspie & Seitz
117 2017). Based on these results, there has been effort to show that the positive relationship between
118 seagrasses and bivalves depends on the surrounding hydrodynamic conditions that alter dispersal
119 and settlement patterns (Eckman 1983, Irlandi 1997). In addition to actively swimming larvae
120 (Koehl & Reidenbach 2007), many benthic invertebrates have planktonic larvae that passively
121 settle in turbulent flow environments (Butman 1989, Koehl & Hadfield 2010). Studies have
122 shown that seagrasses may trap these passive larvae just as they trap sediment and that bivalve
123 settlement patterns may be associated with seagrass presence and canopy structure which alters
124 flow (Eckman 1983, Bologna & Heck 2002).

125 Bay scallops (*Agropecten irradians*) for example, have an extremely close association to
126 seagrass beds by nature of their settlement method (Carroll et al. 2012). Eckman (1987) studied
127 the influence of hydrodynamic forces on recruitment, growth, and survival of bay scallops,
128 concluding that the altered hydrodynamics of eelgrass (*Z. marina*) beds significantly affected

129 larval recruitment to a higher degree than predation or inter-blade abrasion. Hydrodynamics also
130 influence the settlement and recruitment of hard clams (*Mercenaria mercenaria*) with increased
131 clam population density and individual growth rates linked to seagrass presence (Peterson et al.
132 1984). The seagrass-induced impact of local hydrodynamics on passively settling larvae
133 explained differences in clam densities between bare and vegetated sites, even when accounting
134 for altered post-settlement survival.

135 Based on these and other studies, landscape ecology has become an increasingly
136 important approach in examining the effects of seagrass on bivalve distribution. Differences in
137 the spatial patterning of a seagrass meadow (in terms of percent cover) can influence the
138 distribution and abundance of faunal inhabitants and alter trophic interactions (McCloskey &
139 Unsworth 2015). The influence of fragmented seagrass habitats on its associated fauna is
140 extremely variable but not always negative as traditionally thought (Carroll et al. 2012), and
141 previous work suggests that fauna along seagrass edges may experience tradeoffs to balance
142 counteracting influences of both enhanced settlement and predation (Bologna & Heck 2002).
143 This may be due to a “settlement shadow” in which, due to the decrease in current speed through
144 a seagrass canopy, particle settlement should be greatest at a canopy edge and decrease into the
145 meadow. This trend was experimentally observed in bivalve larvae by Bologna & Heck (2000)
146 who found significantly greater larval densities at seagrass patch edges.

147

148 1.4 Seagrass fragmentation and landscape dynamics

149 Anthropogenic influence from coastal development and a simultaneously warming
150 climate have accelerated the rate of seagrass ecosystem loss (Dunic et al. 2021). This degradation

151 drives not only ecosystem loss, but also fragmentation, leading to a more discontinuous habitat
152 (Yarnall et al. 2022). While the natural edges of seagrass meadows have previously been viewed
153 as a ‘presence vs absence’ dichotomy of vegetation, the increased prevalence of edges across
154 fragmented seagrass ecosystems can impact hydrodynamics and sediment movement on both
155 small and large spatial scales (Colomer et al. 2017, Zhu et al. 2022). However, research
156 addressing varied seagrass landscape structure at a range of scales has yielded inconsistent
157 results regarding the relationships between flow regime, sediment transport, and faunal
158 distribution. There remain unanswered questions into how these dynamics persist over a variety
159 of edge settings including that of a homogeneous meadow, or those which characterize
160 fragmented or heterogeneous landscapes. This research therefore addresses the following
161 questions: (1) How do hydrodynamic conditions and wave activity change across edges of
162 seagrass vegetation at the meadow scale and in fragmented landscapes? (2) How do these altered
163 flow conditions influence sediment deposition and transport? (3) Does bivalve settlement and
164 recruitment vary in response to these flow changes?

165

166 2. MATERIALS & METHODS

167 2.1 Study Site

168 Field studies were conducted in South Bay, a coastal lagoon set behind barrier islands
169 bordering the east side of the Delmarva Peninsula, Virginia, USA (Figure 1). This shallow bay is
170 part of the National Science Foundation’s Virginia Coast Reserve Long Term Ecological
171 Research (VCR LTER) site that consists of several coastal bays and their interconnected salt
172 marshes, ocean inlets, and barrier islands. South Bay has an approximate area of 31.5 km² with
173 an average depth of roughly 1.0 m and a tidal range between 0.5 and 1.5 m (Reidenbach &

174 Thomas 2018). Due to the shallow depth, low freshwater inputs, and narrow ocean channels into
175 South Bay, turbidity is primarily caused by sediment resuspension induced by wind-driven
176 waves and transport driven by tidal currents (Lawson et al. 2007, Fagherazzi & Wiberg 2009).
177 High concentrations of resuspended sediment may limit light penetration through the water
178 column with resulting decreases in primary productivity (McGlathery et al. 2001).

179 The shallow coastal lagoons of the Delmarva Peninsula were once dominated by *Zostera*
180 *marina* eelgrass. A combination of disease and extreme weather in the early 1930s led to local
181 elimination of *Zostera marina*. However, when natural occurrences of *Z. marina* were
182 discovered in the 1990s, systematic restoration efforts began in several coastal bays including
183 South Bay and this work has been largely successful with continued meadow reseeding and
184 growth (Oreska et al. 2021). Seeds were initially broadcasted in South Bay in 0.4 ha plots,
185 beginning in 2001, and over subsequent years coalesced into a continuous meadow of 7 km² as
186 of 2015. However, a large seagrass-die off occurred in 2015, linked to a marine heat wave (Aoki
187 et al. 2021), which has altered the spatial distribution of the meadow and impacted seagrass
188 restoration success. Seagrass recovery has subsequently occurred in South Bay, and meadow
189 expansion continues to change the fluid dynamics within this system (Reidenbach & Thomas
190 2018). Seagrasses within the system typically reach a maximum shoot density of >500 shoots m⁻²
191 in early summer and a minimum of 50-100 m⁻² during winter senescence (Berger et al. 2020).

192 In 2021 a study area Site 1 was selected on the northern edge of the South Bay eelgrass
193 meadow (Figure 1B). Three replicate transects were delineated along a 130° trajectory roughly
194 perpendicular to the dominant north-south flow direction of South Bay. Each transect had four
195 sampling locations (A-D) for sediment, bivalve and hydrodynamic conditions with (A) in
196 naturally unvegetated seafloor, (B) 5 m from the vegetation edge within meadow, and (D) 25 m

197 from the vegetation edge within meadow. All sampling locations labeled (C) were located within
198 a patch of bare seafloor where seagrass was manually removed from a circular area 3 m diameter
199 and located 15 m from the seagrass edge (Figure 1B). This sampling location C was used to
200 simulate fragmentation and address how bare patches and edges of discontinuous seagrass cover
201 contribute to alterations of local flow conditions and sediment dynamics. Site 1 was
202 characterized as having a dense seagrass cover which ranged from 480 to 680 shoots m⁻² during
203 sampling, with an average of 555 ± 75 shoots m⁻².

204 In 2022 a second study area, Site 2, was chosen to conduct additional sampling at a
205 region within the canopy considered to have low seagrass density, ranging between 150 and 245
206 shoots m⁻² during time periods of sampling, with an average of 200 ± 50 shoots m⁻². On average,
207 blade length was 48 ± 8 cm and blade width was 0.35 cm with submerged canopy height
208 approximately 30 cm. The canopy was consistently subtidal with average water depth across
209 sites and sampling periods ranging between 1.04 and 1.95 m and low tide depths approximately
210 0.5 m. Site 2 was located approximately 100 m to the northeast of Site 1 and similarly positioned
211 along the northern edge of the South Bay seagrass meadow (Figure 1). One transect was
212 delineated at Site 2 with three designated sampling locations (A, B, and E). Location A was in
213 naturally bare seafloor 5 m from the edge, location B was within the seagrass meadow 5 m from
214 the edge, similar to Site 1. A third location E was located 100 m into the seagrass canopy. This
215 transect ran roughly perpendicular to the meadow's edge in this location (along a 150° trajectory)
216 and along South Bay's dominant flow direction. No bare patches were created at Site 2, but
217 repeated sampling was performed at Site 1 in 2022 at all four locations.

218

219 2.2 Hydrodynamic Instrumentation

220 To assess differences in wave characteristics across the meadow's edge, wave gauges
221 (Richard Branker Research RBRduo³) were concurrently deployed during multiple two to three
222 week deployments, for nearly continuous recordings from May through August 2021 at Site 1.
223 These instruments were fastened to weighted metal frames 10 m apart, one positioned in the
224 naturally bare seafloor at location A and one in full vegetation at location B. To maximize data
225 quality with battery and instrument memory limitations, instruments were programmed to record
226 wave height measurements every 10 minutes at 4 Hz for bursts of 1024 samples (i.e., 256
227 seconds of data) which were averaged to produce a mean value every 10 minutes. Measurements
228 include water depth, tidal slope, and significant wave height. These instruments were again
229 deployed in summer 2022 at site 2 in locations A and B.

230 Two high resolution Nortek Aquadopp acoustic Doppler current profilers (ADCPs) were
231 used to quantify flow conditions in 2021 at Site 1 in bare and vegetated sampling locations (A
232 and D), and in 2022 at Site 2 (locations A and E). Instruments were positioned on the seafloor at
233 $z = 5$ cm in an upward looking orientation and attached to the same frames as the RBRduo³
234 instruments. The ADCPs were programmed to collect velocity data every 10 minutes at 2 Hz for
235 a burst of 60 samples (i.e., 30 seconds of data) in 0.03 m bins starting roughly 0.1 m above the
236 seafloor from May through August 2021 and 2022. An approximately 30 cm diameter section of
237 seagrass was removed surrounding the Aquadopp sensors to prevent interference with flow
238 measurements. Using the internal instrument compass and tilt sensors, velocity measurements
239 were recorded in the east-north-up (ENU) coordinate system to produce both directional and
240 horizontally averaged velocity profiles in 0.03 m bin elevations from $z = 0.1$ m to roughly $z = 1.5$
241 m (upper boundary due to instrument limit). Due to signal interactions with the water surface,
242 velocities within 0.2 m of the water surface were not recorded. To determine the impacts of

243 seagrass on mean flow structure, velocities at the top of the canopy ($z=0.3$ m) were compared to
244 velocities above the canopy ($z=0.6$ m) as well as comparison at these two elevations from within
245 and outside the canopy.

246 A Nortek Vectrino II acoustic Doppler velocimeter was deployed along two transects at
247 Site 1 to quantify changes in flow and turbulence conditions across various edges of vegetation.
248 The longer edge transect covered 10 meters, beginning 5 m away from the seagrass edge over a
249 naturally bare seafloor, with the edge of vegetation as the transect midpoint, and continuing 5
250 more meters into full vegetation past the edge. Velocity data was collected at 10 sampling
251 locations in 1m increments along the transect, which was located immediately west of the
252 manmade bare patches. The shorter patch transect spanned 3 meters beginning in the center of
253 the manmade bare patch (C), crossing the edge of vegetation, and continuing 1.5 meters into the
254 seagrass. Data was collected at 7 sampling locations in 0.5-meter increments along this transect.
255 These distances were chosen to best quantify flow modification by the seagrass edge and patch
256 over a time period where tidal and wave conditions wouldn't change appreciably from start to
257 finish of a transect. At each transect sampling location, the Vectrino was attached to an immobile
258 frame in a downward facing orientation to record velocity data at an elevation of $z = 0.1$ m above
259 the seafloor at 25 Hz for 5 minutes, resulting in 7500 samples at each location on the transects. If
260 necessary, a small 10 cm diameter circular area of seagrass was removed to prevent interference
261 with the Vectrino flow measurements. Four Vectrino transect deployments occurred with water
262 velocities and H_s for each deployment shown in Table 1.

263 In summer 2022 two Nortek Vector acoustic Doppler instruments were deployed at Site
264 2, located 10 m apart, each at 5 m from the natural edge of seagrass vegetation at locations A and
265 B. This distance was chosen to mimic the overall transect distance of the Vectrino data at Site 1.

266 The Vectors were placed downward facing on frames to collect data at z=0.1 m. The instruments
267 recorded data for 72 hours per deployment, recording data every 20 minutes for a burst of 10-
268 minute duration at a sampling rate of 32 Hz.

269 Meteorological data were obtained from a nearby NOAA Station (WAHV2 – 8631044)
270 in Wachapreague, VA where wind speed (m/s) and direction were measured every six minutes.

271

272 2.3 Hydrodynamic data analysis

273 Both the Nortek Vectrino and Vector collect horizontal (u), transverse (v), and vertical
274 velocities (w). Velocity components are separated due to their contributions to mean currents,
275 turbulence, and waves by utilizing the phase method of spectral decomposition (Bricker &
276 Monismith, 2007). For example, the horizontal component of instantaneous flow (u) can be
277 expressed as:

$$278 \quad u = u' + \tilde{u} + \bar{u} \quad (1)$$

279 where u' is the turbulent velocity, \tilde{u} is wave induced orbital velocity and \bar{u} is the mean velocity.

280 Following the decomposition methodology, the mean velocity (\bar{u}) is first subtracted from the
281 instantaneous velocities, and the power spectral densities (PSD) of the remaining fluctuating
282 components of the velocities are computed. Larger values of spectral density correspond to a
283 higher magnitude of energy in the flow for a given frequency, and integrating the area under the
284 curve quantifies the magnitude. Generally, $0.3 < f < 2$ Hz encompass motions from the wave
285 band and are identified within the spectra, then separated from that of mean flow and turbulence
286 by quantifying a best-fit $-5/3$ slope line to the inertial subrange outside of the wave band (Hansen
287 & Reidenbach 2012). Under spectral decomposition theory, spectral energy above the $-5/3$
288 inertial subrange fit is due to wave energy, while that below the fit is due to turbulent energy.

289 This same technique is applied in the same way separately to the u , v , and w velocity
 290 components. This method of decomposition allows for the quantification of turbulent Reynolds
 291 stress (TRS) as:

$$292 \quad \overline{u'w'} = \overline{uw} - \overline{\tilde{u}\tilde{w}} \quad (2)$$

293 Further information regarding this method as applied in vegetated flows can be found in
 294 Hansen & Reidenbach (2012). Turbulent kinetic energy (TKE) is then quantified as:

$$295 \quad TKE = 0.5(\overline{u'^2} + \overline{v'^2} + \overline{w'^2}) \quad (3)$$

296 Linear wave theory was used to quantify wave orbital velocities from water pressure data
 297 collected by the Vector's pressure sensor (Hansen & Reidenbach 2012). The spectral density of
 298 surface elevation, $S_{\eta\eta p}$, is computed as:

$$299 \quad S_{\eta\eta p} = \left[\frac{\cosh(kh)}{\cosh(kz)} \right] \frac{S_{pp}}{\rho^2 g^2} \quad (4)$$

300 where S_{pp} is the spectral density of the pressure, k is the wave number, h is the mean water depth,
 301 z is the height of the pressure sensor above the bottom, g is gravitational acceleration and ρ is
 302 density (Dean & Dalrymple 1991). Significant wave height (H_s) and average period (T) are then
 303 computed using the first ($m0$) and second ($m2$) moments from the $S_{\eta\eta p}$ power spectrum:

$$304 \quad H_s = 4\sqrt{m0} \quad T = \sqrt{m0/m2} \quad (5)$$

305 Where $m0 = \int S_{\eta\eta p}(f)df$ and $m2 = \int f^2 S_{\eta\eta p}(f)df$. The horizontal component of orbital
 306 velocity, u_o , can then be computed as:

$$307 \quad u_o = \frac{\pi H_s}{\sqrt{2}T} \frac{\cosh(kz)}{\sinh(kh)} \quad (6)$$

308 Assuming linear wave theory, the frequencies at or above which wave attenuation will occur at a
309 given elevation z above the seafloor and in water depth h is given as (Wiberg & Sherwood
310 2008):

$$f > \sqrt{g/[4\pi(h - z)]} \quad (7)$$

312 All statistical analyses (ANOVA, t-test, correlation tests) performed on hydrodynamic data were
313 conducted in R version 4.2.2. Hydrodynamic calculations were conducted in Matlab version
314 R2021a.

315

316 2.4 Sediment sampling

317 The previously mentioned wave gauges (RBRduo³) also contained turbidity sensors, and
318 were deployed in summer 2021 and 2022 for the same time periods, from May through August
319 2021 and 2022, and at the same locations as Aquadopp instrumentation. The sensors were
320 programmed to measure in Nephelometric Turbidity Units (NTUs) every ten minutes at 4 Hz for
321 a one-minute burst. In summer 2022, SSCs were also quantified using an optical backscatter
322 sensor (OBS; Campbell Scientific OBS3+) connected to each Vector and housed on the same
323 instrument frame to collect data concurrently. Values of NTU measured by the OBSs were
324 converted to SSCs with units of mg/L using previously calculated calibration values (Hansen &
325 Reidenbach 2012), performed on the same instruments and with sediment from the South Bay
326 seagrass meadow.

327 Sediment traps were used to measure deposition of sediment at Sites 1 and 2 (Figure 2).
328 The trap dimensions formed a 4:1 aspect ratio of internal length to internal diameter which has
329 been deemed appropriate for lower energy systems (Storlazzi et al. 2011). The trap designs were
330 adapted from Wilson 1990, and constructed of 7.6 cm diameter PVC Charlotte piping, cut to a

331 30.5 cm length. Pipe caps (Charlotte Co.) were used to seal the bottom ends of the traps
332 preventing sediment loss and allowing minimal water drainage. The traps were placed within
333 PVC “sleeves” which provided an easier method for frequent removal and replacement instead
334 of continually redeploying into the sediment (Wilson 1990). Sleeves were made from PVC
335 Charlotte Pipe of 10.2 cm diameter with a length of 28 cm. The sleeves were deployed into the
336 sediment with an extension of 10 ± 2 cm above the seafloor where they remained for the study
337 period. This resulted in a final total trap height between 10 and 15 cm above the seafloor. To
338 avoid faunal interference, a polypropylene mesh (6 mm mesh size) covered the trap’s opening.
339 Considering the spacing guidelines described by Storlazzi et al. (2011), traps were deployed at
340 Sites 1 and 2 where each transect location had 3 replicates spaced 1 m apart, yielding a total of
341 12 traps per deployment at Site 1 in 2021 at locations A-D (at the transect furthest to the North),
342 and 9 traps at Site 2 in 2022 at locations A, B, and E. Traps were exchanged roughly every two
343 weeks. Trap contents were emptied into pre-weighed aluminum bins and any fauna collected
344 were removed. Remaining sediment contents were dried at 60° C for at least 24 hours and
345 measured again for a final dry weight. This weight was divided by days of data collection and
346 trap opening area to produce a total collection rate per area (g/cm²/day). All statistical analyses
347 (ANOVA, t-test, correlation tests) performed on sediment data were conducted in R version
348 4.2.2.

349
350 2.5 Bivalve sampling
351 Sediment cores of 7.6 cm diameter were taken from the top 5 cm of sediment roughly
352 every week from June through August 2021 at Site 1. Samples were taken at each of the 12 total
353 locations (A-D) within a 3 m diameter adjacent to the sediment trap replicates. All contents were

354 immediately bagged and placed on ice for transport to the laboratory where they were
355 refrigerated and then processed within 48 hours of collection. All samples were wet-sieved
356 through a 500 μm mesh and remaining contents were examined without magnification and with a
357 dissecting microscope. An identification key was used to distinguish ambiguous specimens and
358 ensure that only bivalves were recorded, but specific species identifications were not performed.
359 A “count” in this methodology represents a bivalve between 500 μm and 1 cm height with its
360 hinge completely maintained and its valves almost entirely intact. Shell fragments or shell hinges
361 with significant weathering were not counted. The final contents were preserved in 70% ethanol
362 and frozen. Two additional rounds of samples were collected and processed in June 2022 at Site
363 1 to assess consistency of results after disturbance generated by creating the manmade bare traps
364 and frequent sampling in summer 2021. A square-root transformation was applied to abundance
365 values to meet assumptions of normality and perform statistical analyses. All statistical analyses
366 (ANOVA, Tukey’s test) performed on bivalve data were conducted in R version 4.2.2.

367

368 3. RESULTS

369

370 3.1 Physical Conditions

371

372 During summer 2021 at Site 1 (mean density of 555 ± 75 shoots m^{-2}), average water
373 depth, as computed from wave gauges, was 1.5 m with tidal fluctuations causing minimum and
374 maximum depths of 0.4 m and 3.0 m. During summer 2022 at Site 2 (mean density of 200 ± 50
375 shoots m^{-2}) average depths at the seagrass site were 1.2 m with minimum depths close to zero
376 during extreme low tides and maximum depths exceeding 2 m. Average monthly wind speeds
377 during summer 2021 ranged from 2.5 ± 0.1 to 4.2 ± 0.1 m/s, with monthly-averaged significant
378 wave height, H_s , at Site 1 within both the bare and seagrass location ranging from 0.05 to 0.10 m.

379 H_s did not differ significantly between the two locations over the entire study period (one-way
380 ANOVA, $F_{1,6} = 0.012$, $p = 0.916$). Maximum $H_s = 0.6$ m occurred during a storm in late May
381 2021, leading to significantly higher H_s averages for the month overall (one-way ANOVA, $F_{3,4} =$
382 274.6, $p < 0.001$). Average wind speed during summer 2022 ranged from 3.4 m/s to 4.7 m/s,
383 with average monthly H_s of 0.07 m, and a maximum during a storm (June 18-20, 2022) with
384 heights exceeding 0.3 m.

385

386 3.2 Mean Flow Conditions

387

388 To address differences in current flow over longer durations of the study period in
389 different sampling locations and across changes in vegetation density, mean velocities
390 throughout the water column were quantified concurrently across Site 1 in seagrass vegetation
391 and along the adjacent bare seafloor. Mean velocities at canopy height ($z=30$ cm) ranged from
392 2.5 to 5.1 cm/s in seagrass vegetation and from 6.8 to 9.1 cm/s over the unvegetated seafloor
393 (Figure 3). Mean velocities in seagrass vegetation were statistically (ANOVA, $F_{1,8} = 42.45$, $p <$
394 0.001) and significantly lower than in adjacent bare areas, with reductions between the two sites
395 ranging from 40% to over 60%. In general, tidal flows and wave propagation followed a roughly
396 North-South orientation creating flows that were parallel to the seagrass edge. There were also
397 statistically significant reductions in velocity at each sampling site comparing elevations of $z=60$
398 cm (above canopy height) to 30 cm ($[100*(U_{z=0.6m} - U_{z=0.3m})/U_{z=0.6m}]$), with seagrass site having up
399 to a 35% decrease in water velocity at the lower elevation (ANOVA, $F_{1,10} = 5.726$, $p = 0.038$),
400 where the bare site only experienced up to a 20% decrease (ANOVA, $F_{1,8} = 8.563$, $p = 0.019$)
401 (Figure 3). Seagrass density peaked in July and corresponded with the season's lowest measured
402 mean velocities of 3.5 cm/s at canopy height ($z = 30$ cm).

403

404 3.3 Hydrodynamic conditions across edges

405

406 In summer 2021, a Vectrino was used to quantify velocities along two transects at Site 1:
407 one a 10 m transect crossing the natural edge of vegetation and the other a 3 m transect covering
408 the manmade bare patch. Data were collected at an elevation of $z = 0.1$ m in 1 m increments
409 along the edge transect and in 0.5 m increments over the patch transect for 5 minutes in each
410 sampling location. Values were averaged into a representative mean for each sampling
411 increment, including velocity magnitude, turbulent Reynolds stress (TRS), and power spectra
412 showing magnitude of energy in the flow at different frequencies. A representative profile of
413 mean velocity and TRS from the patch transect is shown in Figure 4 along with the
414 corresponding PSD from unvegetated and vegetated sampling locations along that transect. Mean
415 velocities were reduced in seagrass by 50% to 75% (Figure 4). Flow energy and associated
416 reductions in vegetation at different frequencies are visualized with PSDs which depict energy
417 magnitude at corresponding frequencies. At almost all frequencies, flow energy in bare areas
418 exceeds that of flows within the vegetation. However, energy from frequencies in the wave band
419 ($0.3 \text{ Hz} < f < 2 \text{ Hz}$) are similar in both sampling locations suggesting that low frequency
420 oscillatory wave energy from wind-generated waves penetrate the seagrass canopy and reach
421 similar magnitude close to the seafloor. Two velocity profiles from the 10 m long edge transect
422 are shown in Figure 5, indicating reductions of mean flow in vegetated areas that exceeded 80%
423 compared to the unvegetated site. Average H_s during both transects was 0.05 m. Overall, mean
424 velocities within the constructed bare patch were lower than those over naturally bare seafloor
425 during the same period of data collection with similar flow and wave conditions.

426 During summer 2022, two Nortek Vector ADVs were concurrently deployed in a
427 stationary (non-profiling) orientation at Site 2, three separate times for a minimum of 72 hours.
428 The instruments were placed 10 m apart, spaced evenly across the natural edge of meadow
429 vegetation. Each of the three deployments were characterized by different physical conditions.
430 Deployment 1 (May 13 – May 16) had the lowest seagrass densities (150 ± 40 shoots/m²) and
431 low-medium wave activity, Deployment 2 (May 23 – May 26) had statistically similar low
432 seagrass densities but the greatest wave activity, and Deployment 3 (June 10 – June 13) had the
433 highest seagrass densities (245 ± 50 shoots/m²) and lowest wave activity. These combinations of
434 meadow morphology and physical setting allowed analysis of how velocity, turbulence, waves,
435 and sediment resuspension respond to different conditions in bare and vegetated areas
436 immediately surrounding a seagrass edge.

437 Depth and H_s data for each deployment are shown in Table 2. Mean velocities at the
438 unvegetated site ranged from 8.8 to 11.1 cm/s and from 3.3 to 7.7 cm/s at the vegetated site. This
439 variability was primarily due to tidal currents. Mean velocities were highest during Deployment
440 1 and decreased with each subsequent deployment, displaying an inverse relationship with
441 seagrass shoot density. Mean velocities were consistently and significantly higher in magnitude
442 at the unvegetated location (two-sided t test, $t_4 = 3.12$, $p = 0.036$). Percent reduction of mean
443 flow speed between the two sampling locations ranged from 30% during Deployment 1 to over
444 65% during Deployment 3, correlating with increases in seagrass shoot density.

445 Turbulent Reynolds stresses were significantly greater in magnitude (Figure 6) at
446 vegetated locations (two-sided t test, $t_4 = -4.55$, $p = 0.011$), ranging from 0.29 to 0.36 cm²/s² at
447 the bare site and from 0.49 to 0.75 cm²/s² in the vegetated site. Wave orbital velocities were
448 quantified at the two sites and ranged between 3.1 and 17.3 cm/s. There were no significant

449 differences in average magnitude between the two sampling locations during each deployment,
450 as indicated by similar H_s between sampling locations. The similarity in wave orbital velocities
451 between sampling locations is also consistent with the similarity in energy from frequencies in
452 the wave band ($0.3 \text{ Hz} < f < 2 \text{ Hz}$) shown in PSDs. Deployment 2 experienced the greatest wave
453 activity caused by elevated wind speeds during this time resulting in the upper limit of measured
454 wave orbital velocities (17 cm/s). Orbital velocities measured during Deployments 1 and 3
455 ranged, on average, between 3 and 4 cm/s and more closely resembled mean flows measured
456 over the duration of the study period.

457 PSDs of vertical velocities measured concurrently at bare and vegetated sites indicate
458 flows were dominated by tidal current during Deployment 1 and by wave activity during
459 Deployment 2 (Figure 7). During tidally dominated flow conditions, a distinct $-5/3$ slope exists in
460 the spectra across 0.2 Hz to 6 Hz frequencies of motion, indicating an expected inertial subrange.
461 Energy magnitude across these frequencies was generally similar between the unvegetated and
462 vegetated sampling locations in this example. During wave-dominated conditions, oscillatory
463 flows due to wave activity adds energy to the turbulent flow, and creates a distinctive peak in the
464 PSD across the wave band ($0.3 \text{ Hz} < f < 2 \text{ Hz}$), disrupting the characteristic $-5/3$ slope of the
465 PSD characterizing the inertial subrange in this region. Outside of the frequencies encompassing
466 the wave band, the same $-5/3$ trend exists. Wave motion effectively penetrated the seagrass
467 canopy, similar to the unvegetated region, as evident by the distinctive peak in the wave
468 frequency band ($0.3 \text{ Hz} < f < 2 \text{ Hz}$).

469 PSDs showing horizontal and vertical velocities for frequencies from 0 to 2 Hz from the
470 bare and vegetated locations are shown for the higher wave conditions during Deployment 2
471 (Figure 8). The black line oscillating across the PSDs portrays the frequency threshold at or

472 above which wave attenuation may be expected due to natural decay of the waves with depth
473 under linear wave theory (Eq. 7). Gaps in data are due to low water levels at low tides leaving
474 the sensors exposed. The data suggest minimal attenuation of wave frequencies ($0.3 \text{ Hz} < f < 2$
475 Hz) in vegetated locations even at relatively high wave activity, but a reduction in low
476 frequencies of $f < 0.3 \text{ Hz}$ in vegetated locations, thus reflecting a reduction in larger, slower
477 turbulent overturns due to drag imposed by the seagrass. It is these lower frequencies ($f < 0.3 \text{ Hz}$)
478 that contribute the majority of the energy to the bulk flow.

479

480 3.4 Sediment suspension and deposition

481

482 Sediment accumulation rates from all sediment trap collection in 2021 are shown in
483 Table 3. Variability between sampling locations remained high, but were statistically similar,
484 with sediment accumulation rates averaged across all sampling dates ranging from 0.56 to 0.74
485 g/cm²/day. The first round of deployment from May 25 to June 2 had sediment collection rates
486 nearly ten times higher than other time periods, likely due to a large storm. To limit variability
487 from this outlier, the spatial groupings were analyzed again excluding the first round of
488 collection. These averages for sites A – D were 0.26, 0.28, 0.37, and 0.27 g/cm²/day respectively
489 (Table 3), which showed lower mean values, but similar trends in deposition when comparing
490 sampling locations. Suspended sediment concentrations (in Nephelometric Turbidity Units:
491 NTU), wind speeds, and H_s were concurrently measured at Site 1, and no significant differences
492 between these values based on their location in bare or vegetated seafloor were found. SSC
493 values were then grouped by month regardless of sampling location to address seasonal changes,
494 and the resulting means are shown in Figure 9 where, like trap collection rates, SSC was elevated
495 in May. Wind speed and wave heights were also elevated and reached their seasonal maximums

496 in late May due to a storm. (Pearson correlation tests between NTU and trap collection rate ($r_2 =$
497 0.986 , $p = 0.014$), NTU and H_s ($r_2 = 0.988$, $p = 0.012$), trap collection rate and H_s ($r_2 = 0.958$, $p =$
498 0.042)). Overall, elevated SSC correlated with higher wind speeds which tended to produce
499 larger wind-driven wave heights, as evident during the May 2021 storm (Figure 10).

500 Rates from all rounds of collection at Site 2 during 2022 are shown in Table 4, where
501 mean rates for sites A, B and E were 0.2 ± 0.02 , 0.29 ± 0.06 , and 0.15 ± 0.02 g/cm²/day
502 respectively, similar to collection rates from 2021. Location B (vegetated location closest to
503 natural edge) had elevated collection rates but statistically similar to location A (in the
504 unvegetated region), while location E (100 m into vegetation away from meadow's edge), had a
505 nearly significant lower collection rate (two-sided t test, $t_{12} = 2.11$, $p = 0.056$). To further
506 address sediment movement across seagrass edges, sediment sensors were deployed at Site 2 in
507 2022 to measure SSCs in the water column at locations A and B, spanning the meadow's natural
508 edge of vegetation. Figure 11 shows the resulting average SSCs with average values between 54
509 and 106 mg/L. Consistent with trap collection data, SSCs were similar to or slightly higher
510 within the vegetated sampling locations 5 m within the seagrass meadow compared to 5 m
511 outside the seagrass meadow. This elevated SSC corresponds to increased turbulent Reynolds
512 stresses measured within the vegetation as compared to outside the vegetation. This suggests that
513 the low canopy density (average of 200 ± 50 shoots/m² for summer 2022) can locally increase
514 near-bed turbulence and SSC concentrations compared to higher canopy densities measured
515 during summer 2021 (average of 555 ± 75 shoots/m²).

516
517 3.5 Bivalve recruitment
518

519 Abundances from all rounds of core sampling during 2021 are shown in Figure 12. A
520 one-way ANOVA and Tukey's test were performed to address differences between core
521 abundances at the four different sampling locations over the entire study period. The groups were
522 statistically different (ANOVA, $F_{3,103} = 22.27$, $p < 0.0001$),) except between groups B and D,
523 indicating that bivalve abundances were lowest in naturally bare areas (A), elevated in the
524 artificial bare patch within the seagrass bed (C), and greatest in areas of full vegetation regardless
525 of edge proximity (B and D). Compared to naturally bare group A, mean abundances were over
526 2.5 times greater in group C and over 4 times greater in groups B and D. A separate one-way
527 ANOVA was performed to address temporal variation with all the sites grouped (Figure 12B).
528 There was high temporal variability with no significant differences in abundance found between
529 June – Sept (ANOVA, $F_{8, 98} = 0.992$, $p = 0.447$).

530 During summer 2022, core samples were collected and processed in the same way at Site
531 1. The removal sites were not cleared again so 2022 samples from location C reflect a year of re-
532 growth, but these locations were still roughly 80% unvegetated. The resulting spatial averages
533 from sampling locations A-D were 1.5, 5.7, 3.2, and 4.7 individuals per core, respectively,
534 statistically similar to those from summer 2021 (Figure 13).

535

536 4. DISCUSSION

537 4.1 Hydrodynamics

538 Wind speeds and significant wave heights were closely correlated (as shown in Figure
539 10), with recorded increases in wind leading to greater H_s and wave orbital velocities. Despite
540 this strong positive relationship between winds and waves, there was no statistical evidence of

541 wave attenuation in seagrass vegetation compared to measurements located at the adjacent
542 naturally bare seafloor. The lack of measurable wave attenuation across this 10 m distance
543 (Table 1) differs compared to previous research that showed measurable attenuation of wave
544 activity over longer spatial distances, with a total decrease of 30% across a 39 m transect of
545 continuous seagrass bed (Bradley & Houser 2009). However, previous work has also shown that
546 unlike unidirectional flow, wave attenuation is not abrupt (Infantes et al. 2012), but may initially
547 increase in significant wave height as waves enter the seagrass bed and subsequently decrease
548 exponentially over the remainder of the bed (Bradley & Houser 2009). Overall, there is an
549 exponential decay rate that can vary in response to the seagrass density and geometry, with wave
550 attenuation increasing as the wave orbital excursion length is increased (Lowe et al. 2005).

551 Longer-period wave motions (including those at tidal periods) can be significantly more
552 attenuated than shorter-period oscillatory motions (Lowe et al. 2007). For the wave heights
553 produced in this study, wave orbital velocities were able to effectively penetrate the seagrass
554 meadow, both at the high seagrass density Site 1 and the low seagrass density Site 2, altering
555 flow dynamics at the seafloor. Our results also indicated that greater flow reduction occurred
556 with increased seagrass blade densities, agreeing with previous research that canopy presence
557 and blade density is responsible for mediating the magnitude current flow attenuation (Koch &
558 Gust 1999, Peterson et al. 2004).

559 Turbulence regimes at Site 1 showed generally reduced Reynolds stresses in seagrass
560 vegetation, but these measurements coincided with high vegetation densities (>500 shoots m^{-2}).
561 Results from summer 2022 reveal opposite trends with greater Reynolds stresses 5 m within the
562 seagrass vegetation within low density regions of the seagrass canopy (<250 shoots m^{-2}). This
563 finding aligns with findings from Hansen & Reidenbach (2012) that turbulent energies can be

564 elevated in vegetated areas of low shoot density due to increased stem-wake interactions in a
565 lower density canopy (Widdows et al. 2008). This increase in turbulence was also reflected in
566 PSDs from the low shoot density Site 2, which showed elevated magnitudes of turbulent energy
567 in seagrass within turbulence frequencies ($> 3\text{Hz}$) of the energy spectra. Measured PSDs at both
568 sites indicate the concurrent decrease in energy at low frequencies ($< 0.3\text{ Hz}$), reflecting a
569 reduction in mean flow. All PSDs revealed similar wave orbital velocities ($0.3\text{ Hz} < f < 2\text{ Hz}$)
570 within seagrass vegetation compared to unvegetated regions across the seagrass edge, suggesting
571 waves effectively penetrate the seagrass canopy that can impact flow interaction with the seabed.

572

573 4.2 Sediment dynamics

574 Sediment trap collection rates and SSC were significantly correlated with each other and
575 with H_s . Winds have previously been shown to be the dominant control on wave activity in this
576 system (Fagherazzi & Wiberg 2009). Wave height was a major predictor in sediment
577 resuspension and transport across these edge settings, and although benthic microalgal
578 concentrations have been shown to impact resuspension rates (Reidenbach & Timmerman 2019),
579 similar wave heights in these locations explain similar levels of sediment movement. Since
580 average grain size diameter is small at $D_{84} < 160\text{ }\mu\text{m}$ (where D_{84} is the sediment grain diameter
581 such that 84% of grain diameters are smaller), once suspended, sediment typically remain in
582 suspension for a few days (Hansen & Reidenbach 2012). Sediment trap collection rates at Sites 1
583 and 2 showed no significant spatial trends across sampling locations within 25 m of the seagrass
584 edge, whether in bare or vegetated areas, or manmade removal areas. However, more notable
585 reductions in sediment deposition occurred at 100 m from the edge (measured at Site 2). This
586 agrees with the work of Zhu et al. (2021 & 2022) who concluded that vegetation density

587 mediates the response of flow along seagrass edges, which creates lower sediment deposition
588 rates along the interior of the meadow relative to deposition rates within ~100 m of edges.
589 Within 25 m of the seagrass edge, high variability from trap collection data could explain
590 statistical similarities in these results, but high resolution, longer-term data sets from optical
591 backscatter sensors were used to concurrently quantify relative levels of SSCs and confirmed
592 nonsignificant differences in turbidity. This suggests that, as seen with wave attenuation
593 (Verduin & Backhaus 2000), a threshold of distance from the meadow's edge may exist for
594 vegetation to reduce SSCs (Zhu et al. 2022), but is likely greater than the ~ 25 m from the edge
595 measured in this study.

596

597 4.3 Bivalve recruitment dynamics

598 Abundances of juvenile bivalves were elevated in all vegetated sampling locations
599 regardless of proximity to edges. Abundances were lower in manmade bare patches and lowest
600 in naturally unvegetated seafloor. These results indicate that seagrass biomass enhance
601 settlement and/or retainment of juvenile bivalves and is consistent with work showing greater
602 bivalve presence in seagrass ecosystems (Orth et al. 1984, Glaspie & Seitz 2017). However,
603 seagrass locations with elevated bivalve abundances also correspond to areas with significant
604 reductions in mean flow. This suggests that the magnitude of the current flow (due to the
605 combined effects of waves and tidal-driven flows) may still mediate bivalve settlement across
606 vegetated locations (Bologna & Heck 2000), and that lower energy flow conditions encourage
607 greater recruitment. The enhanced recruitment, therefore, may be due to the benefits of a
608 reduction in flow forces imposed on settling larvae (Reidenbach et al. 2009, Reidenbach et al.
609 2021) and decreased mortality and predation (Orth et al. 1984, Boström et al. 2010) through

611 sheltering by the seagrass canopy. Previous research has shown significant wave attenuation at
612 more interior locations of the seagrass bed (Thomas & Reidenbach 2018), which may also
613 impact bivalve recruitment. However, along the edges of seagrass measured in this study, no
614 significant change in wave oscillations were measured within and outside the meadow, therefore
615 the effects of waves on bivalve recruitment could not be determined.

616 Of note is the strong impact that seagrass edges have on bivalve recruitment, but a much
617 weaker response to sediment deposition dynamics. This may be due to the more active
618 swimming behaviors of some settling larvae which can alter settlement locations to a much
619 greater degree (Abelson & Denny 1997, Koehl & Reidenbach 2007) than passive sediment
620 particles. However this direct effect of larval behaviors on settlement dynamics within seagrass
621 systems has not been studied.

622

623 4.4 Conclusions

624

625 The results presented here indicate that over various edges of heterogenous vegetation
626 along different spatial configurations, mean velocities were consistently and significantly
627 reduced in seagrass vegetation, and negatively correlated with increased shoot density. However,
628 over these short spatial distances of < 10 m, there was no evidence of wave attenuation or within-
629 canopy wave orbital velocities in any of the vegetated locations. Interestingly, along edges of
630 vegetation, Reynolds stresses were elevated in seagrass vegetation in low density regions,
631 indicating a higher level of turbulent energy presumably due to increased stem-wake interactions
632 (Nepf et al. 1997, Widdows et al. 2008), the magnitude of which depends upon the flexibility of
633 the blades and if vegetation is emergent or submerged. Although these findings generally agree

634 with previous laboratory and field measurements of wave attenuation and turbulence (Bradley &
635 Houser 2009, Infantes et al. 2012) for submerged and flexible vegetation, our study addressed
636 how these changes impact sediment and bivalve settlement.

637 Our findings suggest that, unlike wave motions, abundances of juvenile bivalves respond
638 rapidly over short spatial distances of < 10 m, with abundances of juvenile bivalves being
639 significantly elevated in seagrass vegetation, presumably due to the sheltering effect caused by
640 seagrass. However, there were no significant changes in turbidity or sediment collection rate at
641 locations within 25 m of the meadow edge, but reduced collection rates were found at 100 m
642 distances. This agrees with previous literature demonstrating reduced SSCs in vegetation across
643 larger spatial scales (Carr et al. 2010, Hansen & Reidenbach 2013). Recent modeling work from
644 South Bay reports that SSCs fluctuate non-linearly as a function of seagrass density and that
645 meadow edges experience the greatest sensitivity to seasonal erosion or deposition due to either
646 mean flows or wave activity while mediating overall advection of SSCs at the meadow scale
647 (Zhu et al. 2022). Flume experiments showed a similar density-dependent relationship between
648 flow regime and distance of sediment deposition past a seagrass edge (Zhang & Nepf 2019). This
649 emphasizes that a minimum threshold of density and/or distance from a meadow's edge may
650 exist to attenuate waves, thus causing a reduction in SSC and sediment deposition, and our
651 findings suggest this distance to be on the scale of 100 m. However, in regions of low wave
652 activity where tidal currents dominate, seagrasses are more effective at reducing flow energy and
653 this distance over which sediment transport is altered should be significantly reduced.

654

655 5. ACKNOWLEDGEMENTS

656 We would like to thank the staff at the Anheuser-Busch Coastal Research Center for
657 assistance in field campaigns. This research was funded by the National Science Foundation
658 grant DEB-1832221 to the Virginia Coast Reserve Long Term Ecological Research project. Data
659 is accessible at: [doi:10.6073/pasta/30de0c4d1086cd7ecb643f5b05c88d8b](https://doi.org/10.6073/pasta/30de0c4d1086cd7ecb643f5b05c88d8b).

660

661 6. LITERATURE CITED

662 Abelson A, Denny MW (1997) Settlement of marine organisms in flow. *Annual Review of*
663 *Ecological Systems* 28:317-339

664 Adams MP, Hovey RK, Hipsey MR, Bruce LC, Ghisalberti M, Lowe RJ, Gruber RK, Ruiz-
665 Montoya L, Maxwell PS, Callaghan DP (2016) Feedback between sediment and light for
666 seagrass: Where is it important? *Limnol Oceanogr*

667 Allen T, Behr J, Bukvic A, Calder RSD, Caruson K, Connor C, D'Elia C, Dismukes D, Ersing R,
668 Franklin R, Goldstein J, Goodall J, Hemmerling S, Irish J, Lazarus S, Loftis D, Luther M,
669 McCallister L, McGlathery K, Mitchell M, Moore W, Nichols CR, Nunez K, Reidenbach
670 M, Shortridge J, Weisberg R, Weiss R, Wright LD, Xia M, Xu K, Young D, Zarillo G,
671 Zinnert JC (2021) Anticipating and Adapting to the Future Impacts of Climate Change on
672 the Health, Security and Welfare of Low Elevation Coastal Zone (LECZ) Communities
673 in Southeastern USA. *Journal of Marine Science and Engineering* 9:1196

674 Aoki LR, McGlathery KJ, Oreska MP (2020) Seagrass restoration reestablishes the coastal
675 nitrogen filter through enhanced burial. *Limnol Oceanogr* 65:1-12

676 Aoki LR, McGlathery KJ, Wiberg PL, Oreska MP, Berger AC, Berg P, Orth RJ (2021) Seagrass
677 recovery following marine heat wave influences sediment carbon stocks. *Frontiers in*
678 *Marine Science* 7:576784

679 Berger AC, Berg P, McGlathery KJ, Delgard ML (2020) Long-term trends and resilience of
680 seagrass metabolism: A decadal aquatic eddy covariance study. *Limnol Oceanogr*
681 65:1423-1438

682 Bologna PA, Heck KL (2000) Impacts of seagrass habitat architecture on bivalve settlement.
683 *Estuaries* 23:449-457

684 Bologna PA, Heck KL (2002) Impact of habitat edges on density and secondary production of
685 seagrass-associated fauna. *Estuaries* 25:1033-1044

686 Boström C, Törnroos A, Bonsdorff E (2010) Invertebrate dispersal and habitat heterogeneity:
687 expression of biological traits in a seagrass landscape. *Journal of Experimental Marine
688 Biology and Ecology* 390:106-117

689 Bradley K, Houser C (2009) Relative velocity of seagrass blades: Implications for wave
690 attenuation in low-energy environments. *Journal of Geophysical Research Earth Surfaces*
691 114:1-13

692 Bricker JD, Monismith SG (2007) Spectral wave-turbulence decomposition. *Journal of
693 Atmospheric and Oceanic Technology* 24(8):1479-1487

694 Butman CA (1989) Sediment-trap experiments on the importance of hydrodynamical processes
695 in distributing settling invertebrate larvae in near-bottom waters. *Journal of Experimental
696 Marine Biology and Ecology* 134:37-88

697 Carr J, D'Odorico P, McGlathery K, Wiberg P (2010) Stability and bistability of seagrass
698 ecosystems in shallow coastal lagoons: Role of feedbacks with sediment resuspension
699 and light attenuation. *Journal of Geophysical Research: Biogeosciences* (2005–2012) 115

700 Carroll JM, Furman BT, Tettelbach ST, Peterson BJ (2012) Balancing the edge effects budget:
701 bay scallop settlement and loss along a seagrass edge. *Ecology* 93:1637-1647

702 Chen SN, Sanford LP, Koch E, Shi F, North EW (2007) A nearshore model to investigate the
703 effects of seagrass bed geometry on wave attenuation and suspended sediment transort.
704 *Estuaries and Coasts* 30:296-310

705 Colomer J, Soler M, Serra T, Casamitjana X, Oldham C (2017) Impact of anthropogenically
706 created canopy gaps on wave attenuation in a *Posidonia oceanica* seagrass meadow. Mar
707 Ecol Prog Ser 569:103-116

708 Donatelli C, Ganju NK, Fagherazzi S, Leonardi N (2018) Seagrass impact on sediment exchange
709 between tidal flats and salt marsh, and the sediment budget of shallow bays. Geophysical
710 Research Letters 45:4933-4943

711 Dunic JC, Brown CJ, Connolly RM, Turschwell MP, Côté IM (2021) Long-term declines and
712 recovery of meadow area across the world's seagrass bioregions. Global Change Biology
713 27:4096-4109

714 Eckman JE (1983) Hydrodynamic processes affecting benthic recruitment. Limnol Oceanogr
715 28:241-257

716 Eckman JE (1987) The role of hydrodynamics in recruitment, growth, and survival of
717 *Argopecten irradians* (L.) and *Anomia simplex* (D'Orbigny) within eelgrass meadows.
718 Journal of Experimental Marine Biology and Ecology 106:165-191

719 El Allaoui N, Serra T, Colomer J, Soler M, Casamitjana X, Oldham C (2016) Interactions
720 between fragmented seagrass canopies and the local hydrodynamics. PLoS ONE
721 11:e0156264

722 Fagherazzi S, Wiberg P (2009) Importance of wind conditions, fetch, and water levels on wave-
723 generated shear stresses in shallow intertidal basins. Journal of Geophysical Research 114

724 Fonseca MS, Koehl MAR (2006) Flow in seagrass canopies: The influence of patch width.
725 Estuar Coastal Shelf Sci 67:1-9

726 Gacia E, Duarte CM (2001) Sediment retention by a Mediteranean *Posidonia oceanica* meadow:
727 the balance between deposition and resuspension. Estuar Coastal Shelf Sci 52:505-514

728 Gambi MC, Nowell AR, Jumars PA (1990) Flume observations on flow dynamics in *Zostera*
729 *marina* (eelgrass) beds. Mar Ecol Prog Ser:159-169

730 Ghisalberti M, Nepf HM (2002) Mixing layers and coherent structures in vegetated aquatic
731 flows. Journal of Geophysical Research 107:3-1 - 3-11

732 Glaspie CN, Seitz RD (2017) Role of habitat and predators in maintaining functional diversity of
733 estuarine bivalves. Mar Ecol Prog Ser 570:113-125

734 Grant WD, Madsen OS (1979) Combined wave and current interaction with a rough bottom.
735 Journal of Geophysical Research 84:1797-1808

736 Hansen JC, Reidenbach MA (2013) Seasonal growth and senescence of a *Zostera marina*
737 seagrass meadow alters wave-dominated flow and sediment suspension within a coastal
738 bay. Estuaries and Coasts 36:1099-1114

739 Hansen JC, Reidenbach MA (2017) Turbulent mixing and fluid transport within Florida Bay
740 seagrass meadows. Advances in Water Resources 108:205-215

741 Hansen JCR, Reidenbach MA (2012) Wave and tidally driven flows in eelgrass beds and their
742 effect on sediment suspension. Mar Ecol Prog Ser 448:271-287

743 Irlandi EA (1997) Seagrass patch size and survivorship of an infaunal bivalve. Oikos:511-518

744 Jing L, Ridd PV (1996) Wave-current bottom shear stresses and sediment resuspension in
745 Cleveland Bay, Australia. Coastal Engineering 29:169-186

746 Koch E, Ackerman JD, Verduin J, van Keulen M (2006) Fluid dynamics in seagrass ecology-
747 from molecules to ecosystems. In: Seagrasses: Biology, Ecology and Conservation.
748 Springer Netherlands, p 193-225

749 Koch E, Gust G (1999) Water flow in tide- and wave-dominated beds of the seagrass *Thalassia*
750 *testudinum*. Mar Ecol Prog Ser 184:63-72

751 Koehl MAR, Hadfield M (2010) Hydrodynamics of larval settlement from a larva's point of
752 view. *Integrative and Comparative Biology* 50:539-551

753 Koehl MAR, Reidenbach MA (2007) Swimming by microscopic organisms in ambient water
754 flow. *Experiments in Fluids* 43:755-768

755 Lawson SE, Wiberg PL, McGlathery KJ, Fugate DC (2007) Wind-driven sediment suspension
756 controls light availability in a shallow coastal lagoon. *Estuaries and Coasts* 30:102-112

757 Lowe RJ, Falter JL, Koseff JR, Monismith SG, Atkinson MJ (2007) Spectral wave flow
758 attenuation within submerged canopies: Implications for wave energy dissipation. *Journal*
759 *of Geophysical Research* 112:C05018, doi:05010.01029/02006JC003605

760 Lowe RL, Koseff JR, Monismith SG (2005) Oscillatory flow through submerged canopies: 1.
761 Velocity structure. *Journal of Geophysical Research* 110:doi:10.1029/2004JC002788

762 Luhar M, Coutu S, Infantes E, Fox S, Nepf H (2010) Wave-induced velocities inside a model
763 seagrass bed. *Journal of Geophysical Research: Oceans* 115

764 McCloskey RM, Unsworth RK (2015) Decreasing seagrass density negatively influences
765 associated fauna. *PeerJ* 3:e1053

766 McGlathery K, Anderson IC, Tyler AC (2001) Magnitude and variability of benthic and pelagic
767 metabolism in a temperate coastal lagoon. *Mar Ecol Prog Ser* 216:1-15

768 McGlathery KJ, Reidenbach MA, D'Odorico P, Fagherazzi S, Pace ML, Porter JH (2013)
769 Nonlinear dynamics and alternative stable states in shallow coastal systems.
770 *Oceanography* 26:220-231

771 Nardin W, Larsen L, Fagherazzi S, Wiberg P (2018) Tradeoffs among hydrodynamics, sediment
772 fluxes and vegetation community in the Virginia Coast Reserve, USA. *Estuar Coast Shelf*
773 *Sci* 210:98-108

774 Nepf HM (2012) Flow and transport in regions with aquatic vegetation. *Annu Rev Fluid Mech*
775 44:123-142

776 Nepf HM, Sullivan JA, Zavistoski RA (1997) A model for diffusion with emergent vegetation.
777 *Limnol Oceanogr* 42(8):1735-1745

778 Nepf HM, Vivoni ER (2000) Flow structure in depth-limited, vegetated flow. *Journal of*
779 *Geophysical Research* 105:28547-28557

780 Oreska MP, McGlathery KJ, Aoki LR, Berger AC, Berg P, Mullins L (2020) The greenhouse gas
781 offset potential from seagrass restoration. *Scientific Reports* 10:1-15

782 Oreska MP, McGlathery KJ, Wiberg PL, Orth RJ, Wilcox DJ (2021) Defining the *Zostera*
783 *marina* (eelgrass) niche from long-term success of restored and naturally colonized
784 meadows: Implications for seagrass restoration. *Estuaries and Coasts* 44:396-411

785 Orth RJ, Heck KL, van Montfrans J (1984) Faunal communities in seagrass beds: a review of the
786 influence of plant structure and prey characteristics on predator-prey relationships.
787 *Estuaries* 7:339-350

788 Peterson CH, Luettich RA, Micheli F, Skilleter GA (2004) Attenuation of water flow inside
789 seagrass canopies of differing structure. *Mar Ecol Prog Ser* 268:81-92

790 Peterson CH, Summerson H, Duncan P (1984) The influence of seagrass cover on population
791 structure and individual growth rate of a suspension-feeding bivalve, *Mercenaria*
792 *mercenaria*. *Journal of Marine Research* 42:123-138

793 Reidenbach MA, Koseff JR, Koehl MAR (2009) Hydrodynamic forces on larvae affect their
794 settlement on coral reefs in turbulent, wave-driven flow. *Limnol Oceanogr* 54:318-330

795 Reidenbach MA, Stocking JB, Szczyrba L, Wendelken C (2021) Hydrodynamic interactions
796 with coral topography and its impact on larval settlement. *Coral Reefs* 40:505-519

797 Reidenbach MA, Thomas EL (2018) Influence of the seagrass, *Zostera marina*, on wave
798 attenuation and bed shear stress within a shallow coastal bay. *Frontiers in Marine Science*
799 5

800 Reidenbach MA, Timmerman R (2019) Interactive effects of seagrass and the
801 microphytobenthos on sediment suspension within shallow coastal bays. *Estuaries and*
802 *Coasts* 42:2038-2053

803 Storlazzi C, Field M, Bothner M (2011) The use (and misuse) of sediment traps in coral reef
804 environments: theory, observations, and suggested protocols. *Coral Reefs* 30:23-38

805 Twomey AJ, O'Brien KR, Callaghan DP, Saunders MI (2020) Synthesising wave attenuation for
806 seagrass: Drag coefficient as a unifying indicator. *Marine Pollution Bulletin* 160:111661

807 Verduin JJ, Backhaus JO (2000) Dynamics of plant-flow interactions for the seagrass *Amphibolis*
808 *antarctica*: Field observations and model simulations. *Estuar Coast Shelf Sci* 50:185-204

809 Wiberg PL, Sherwood CR (2008) Calculating wave-generated bottom orbital velocities from
810 surface-wave parameters. *Computers and Geosciences* 34:1243-1262

811 Widdows J, Pope ND, Brinsley MD, Asmus H, Asmus RM (2008) Effects of seagrass beds
812 (*Zostera noltii* and *Z. marina*) on near-bed hydrodynamics and sediment resuspension.
813 *Mar Ecol Prog Ser* 358:125-136

814 Wilson FS (1990) Temporal and spatial patterns of settlement: a field study of molluses in Bogue
815 Sound, North Carolina. *Journal of Experimental Marine Biology and Ecology* 139:201-
816 220

817 Yarnall AH, Byers JE, Yeager LA, Fodrie FJ (2022) Comparing edge and fragmentation effects
818 within seagrass communities: A meta-analysis. *Ecology* 103:e3603

819 Zhang Y, Nepf H (2019) Wave-driven sediment resuspension within a model eelgrass meadow.

820 Journal of Geophysical Research: Earth Surface 124:1035-1053

821 Zhu Q, Wiberg PL, McGlathery KJ (2022) Seasonal growth and senescence of seagrass alters

822 sediment accumulation rates and carbon burial in a coastal lagoon. Limnol Oceanogr

823 67:1931-1942

824 Zhu Q, Wiberg PL, Reidenbach MA (2021) Quantifying Seasonal Seagrass Effects on Flow and

825 Sediment Dynamics in a Back-Barrier Bay. Journal of Geophysical Research: Oceans

826 126:e2020JC016547

827

828 7. TABLES

829

830

831 **Table 1.** Average water velocities (cm/s) and H_s (m) from the four Vectrino deployments along the two
832 Site 1 transects during summer 2021. Water velocities and H_s quantified at the beginning (unvegetated)
833 and ending (vegetated) locations of each transect.

| | Velocity (unvegetated, cm/s) | Velocity (vegetated, cm/s) | H_s (unvegetated, cm) | H_s (vegetated, m) |
|----------------------|---------------------------------|-------------------------------|----------------------------|----------------------|
| <i>July 15 Patch</i> | 5.7 | 1.4 | 4.4 | 3.7 |
| <i>July 26 Edge</i> | 6.2 | 1.4 | 3.2 | 5.0 |
| <i>Aug 10 Edge</i> | 13.3 | 1.8 | <1.0 | <1.0 |
| <i>Aug 18 Patch</i> | 4.4 | 2.0 | <1.0 | <1.0 |

834

835

836

837

838 **Table 2.** Average and maximum of water depth \pm 1 SE (m) and significant wave height \pm 1 SD, H_s (m),
839 from the unvegetated and vegetated sampling locations of the three Vector deployments at Site 2 during
840 summer 2022. Water depths were statistically different between unvegetated and vegetated sites within a
841 given deployment, but H_s was not statistically different.

| | Deployment 1: 5/13 – 5/16 | | Deployment 2: 5/23 – 5/26 | | Deployment 3: 6/10 – 6/13 | |
|-----------------------------|---------------------------------|-------------------------------|---------------------------------|-------------------------------|---------------------------------|-------------------------------|
| <i>Avg Depth</i> | Unvegetated 1.04 \pm 0.014 | Vegetated 0.90 \pm 0.014 | Unvegetated 1.20 \pm 0.007 | Vegetated 1.09 \pm 0.007 | Unvegetated 0.97 \pm 0.007 | Vegetated 0.89 \pm 0.007 |
| <i>Max Depth</i> | 1.95 | 1.78 | 1.92 | 1.83 | 1.86 | 1.78 |
| <i>Avg H_s</i> | 0.06 \pm 0.06 | 0.06 \pm 0.06 | 0.14 \pm 0.08 | 0.16 \pm 0.08 | 0.04 \pm 0.04 | 0.05 \pm 0.04 |
| <i>Max H_s</i> | 0.14 | 0.16 | 0.32 | 0.32 | 0.09 | 0.11 |

842

843

844

845 **Table 3.** Sediment trap accumulation rates (g/cm²/day) from 2021 at Site 1 where the three replicates
 846 from each sampling location (A-D) are averaged into one value for that round of data collection. Bottom
 847 two rows show the total mean of that sampling location over the study period \pm 1 SE both including and
 848 excluding the elevated first round of trap collection (Rd1) in late May. Location A was located in the
 849 unvegetated seafloor 5 m from seagrass edge, B was 5 m from the edge within the seagrass meadow, C
 850 was a manmade bare patch 15 m from the edge, and D was located 25 m from the edge within the
 851 meadow.

852

| <i>Collection Dates (2021)</i> | <i>A</i> | <i>B</i> | <i>C</i> | <i>D</i> |
|--------------------------------|-----------------|-----------------|-----------------|-----------------|
| <i>May 25 – June 2</i> | 2.86 | 2.61 | 2.73 | 2.03 |
| <i>June 2 – June 16</i> | 0.32 | 0.17 | 0.35 | 0.25 |
| <i>June 18 – June 29</i> | 0.36 | 0.32 | 0.28 | 0.18 |
| <i>June 29 – July 10</i> | 0.21 | 0.20 | 0.26 | 0.23 |
| <i>July 27 – Aug 9</i> | 0.12 | 0.22 | 0.21 | 0.19 |
| <i>Aug 9 – Sept 10</i> | 0.13 | 0.19 | 0.44 | 0.19 |
| <i>Sept 10 – Oct 12</i> | 0.44 | 0.65 | 0.66 | 0.59 |
| <i>Mean incl. Rd1</i> | 0.67 ± 0.24 | 0.65 ± 0.2 | 0.74 ± 0.22 | 0.56 ± 0.16 |
| <i>Mean excl. Rd1</i> | 0.26 ± 0.05 | 0.28 ± 0.08 | 0.37 ± 0.07 | 0.27 ± 0.07 |

853

854

855

856 **Table 4.** Sediment trap accumulation rates (g/cm²/day) from 2022 at Site 2 where the three replicates
 857 from each sampling location (A, B, and E) are averaged into one value for that round of data collection.
 858 Location A was located in the unvegetated seafloor 5 m from seagrass edge, B was 5 m from the edge
 859 within the seagrass meadow, and E was located 100 m from the edge within the meadow.

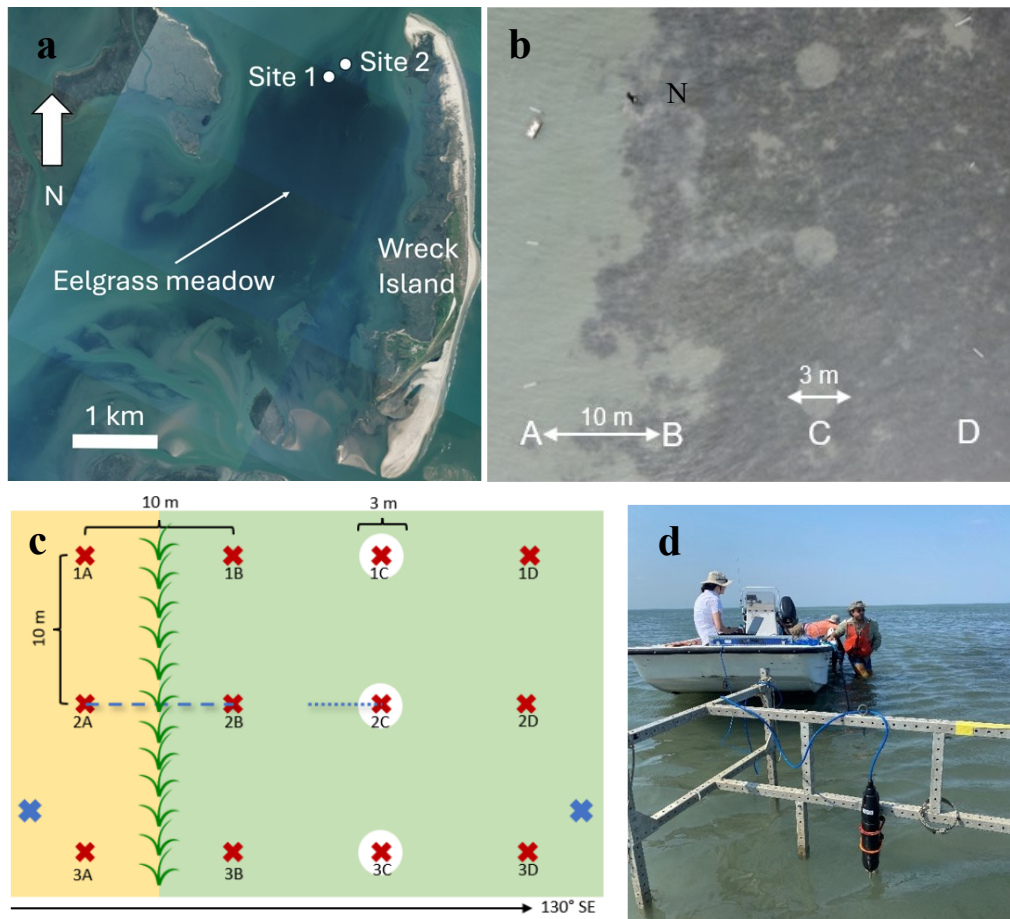
860

861

| <i>Collection Dates (2022)</i> | <i>A</i> | <i>B</i> | <i>E</i> |
|--------------------------------|-----------------|-----------------|-----------------|
| <i>May 13 – May 26</i> | 0.28 | 0.43 | 0.18 |
| <i>May 26 – June 10</i> | 0.13 | 0.14 | 0.08 |
| <i>June 10 – June 30</i> | 0.19 | 0.37 | 0.17 |
| <i>Mean</i> | 0.20 ± 0.02 | 0.29 ± 0.06 | 0.15 ± 0.02 |

862

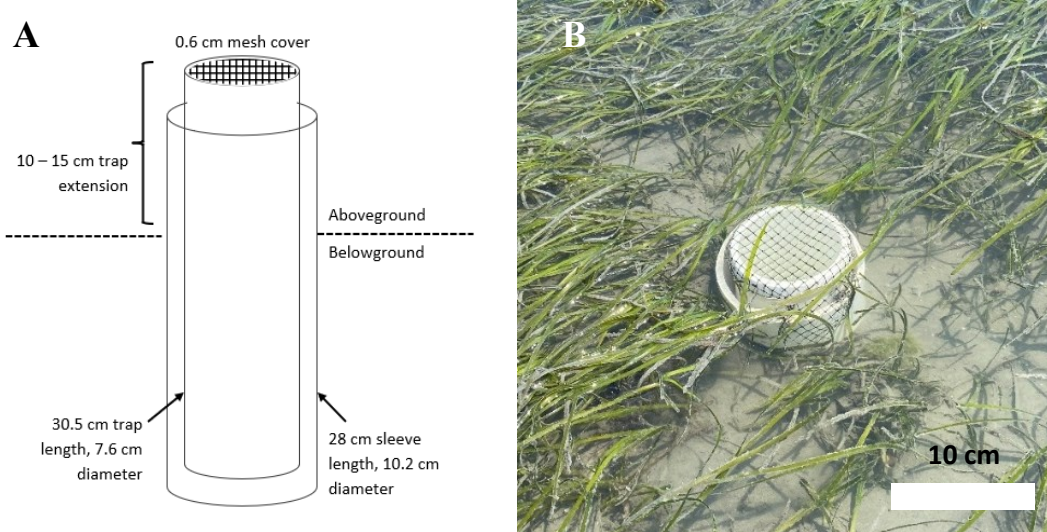
863



866 **Figure 1.** (a) Aerial image of study locations Site 1 (37.278611 N, -75.811389 W) and Site 2 (37.279167
 867 N, -75.810833 W) along the northern edge of South Bay eelgrass
 868 meadow can be seen as dark regions within the bay, to the west of Wreck barrier island (b) Aerial photo
 869 of Site 1 showing four sampling locations (A – D) along three parallel transects, including manmade bare
 870 patches at locations 'C'. (D) Schematic of Site 1 sampling array with three parallel transects (1-3) heading
 871 130° SE from naturally unvegetated seafloor (yellow) past the meadow's edge into vegetation (green),
 872 each with four replicative, designated locations (A-D) for bivalve and sediment sampling (red Xs). Site
 873 1C locations occur in manmade bare patches of 3 m diameter (white). Hydrodynamic sampling occurred
 874 along smaller transects and at site perimeters (blue dashes, blue Xs). (E) Image of Vectrino on frame used
 875 to compute transect velocities.

879

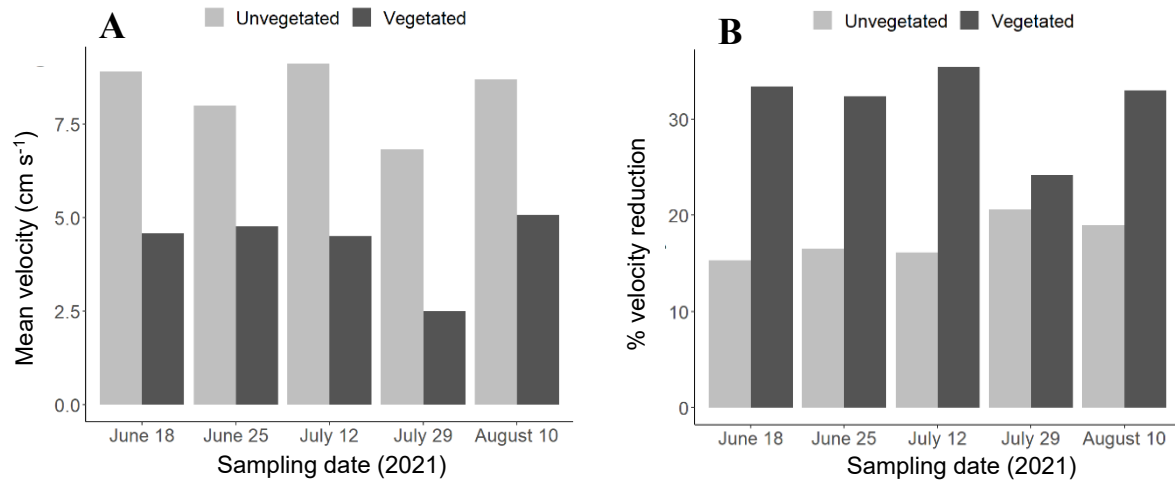
880



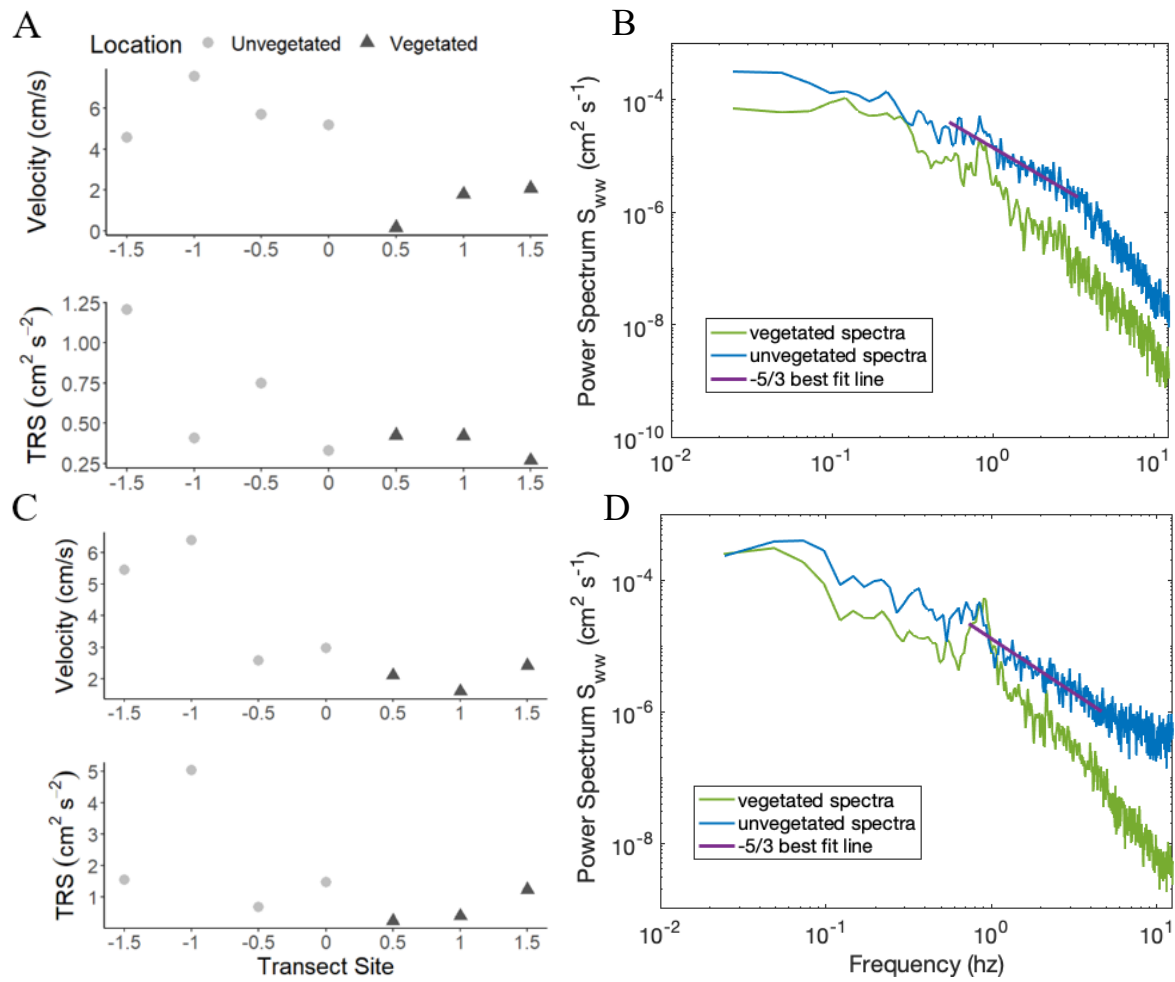
881

882 **Figure 2.** (Left) Schematic diagram of PVC sleeve and trap design adapted from Wilson (1990), not to
883 scale. (Right) Photo of sleeve and trap system deployed *in situ*.

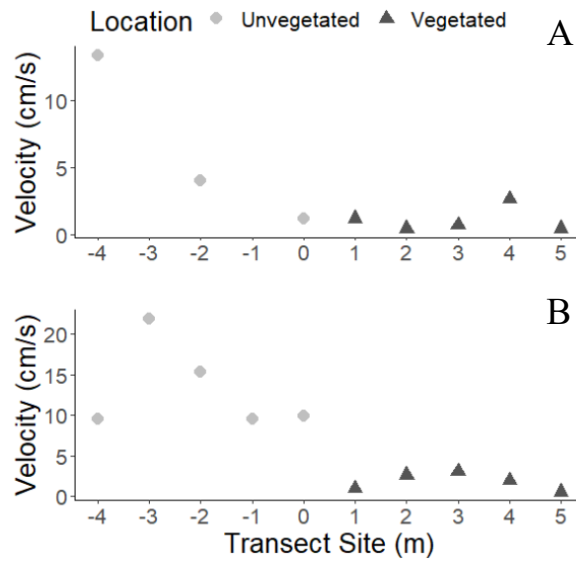
884



887 **Figure 3.** A) Mean velocities (cm/s) quantified at a $z=30$ cm elevation above the seafloor for each
 888 deployment period of 2021 from unvegetated (light) and vegetated (dark) sampling locations. B) Percent
 889 velocity reduction from $z=60$ to 30 cm elevations in the water column [$100*(U_{z=0.6m}-U_{z=0.3m})/U_{z=0.6m}$],
 890 at vegetated and unvegetated sampling locations.



895 **Figure 4.** Profiles of mean velocity (cm/s) and turbulent Reynolds stress (cm²/s²) at z= 0.1 m from
 896 transects spanning the manmade bare patch on (A) July 15, 2021 and (C) August 18, 2021 and PSDs from
 897 the same dates (B and D, respectively) quantified in unvegetated (yellow) and vegetated (blue) sampling
 898 locations. The -5/3 slope lines shown in each graph indicates the best fit to the inertial subrange of the
 899 turbulence. Significant wave height during both sampling times were ~0.05 m. Distance between transect
 900 sites is 0.5 m and seagrass edge begins between site 4 and 5. Mean wind and flow conditions for the
 901 transects shown are included in Table 1.



903

904

905 **Figure 5.** Profiles of mean velocity (cm/s) at $z = 0.1$ m from transects spanning the meadow's natural edge
 906 of vegetation on (A) July 26, 2021 and (B) August 10, 2021. Distance between transect sites is 1m, and
 907 the meadow edge begins at 0 m. Mean wind and flow conditions for the transects shown are included in
 908 Table 1. Due to instrument error no data was collected at transect site -4 or -2 m on July 26, 2021.

909

910

911

912

913

914

915

916

917

918

919

920

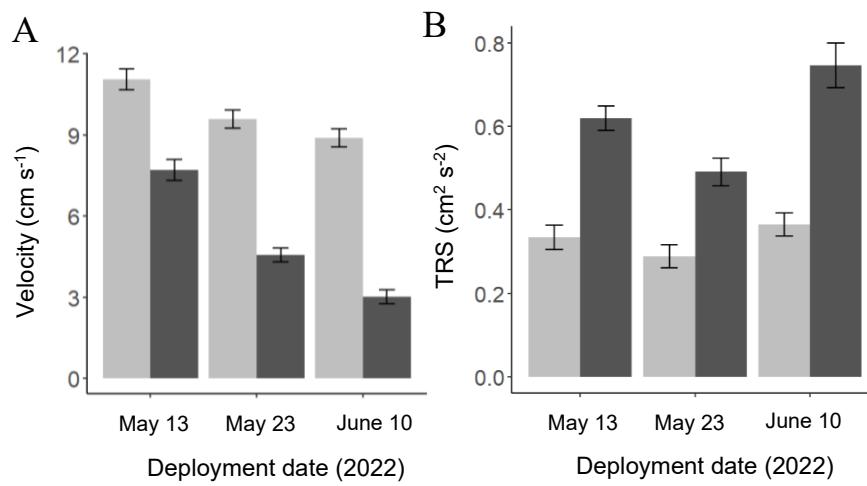
921

922

923

924

925

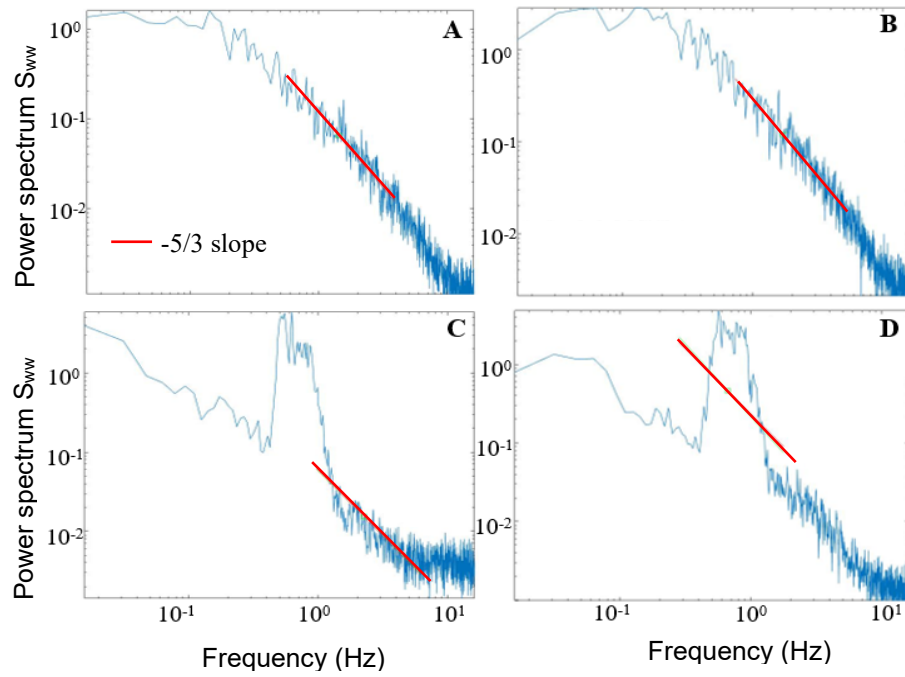


926

927 **Figure 6.** A) Mean velocities ± 1 SE and B) turbulent Reynolds stresses ± 1 SE shown from unvegetated
928 and vegetated sampling locations during the three Vector deployments in 2022 (May 13, 23 and June 10,
929 2022).

930

931



932

933 **Figure 7.** Power spectral densities (PSD) of vertical velocity energy magnitude from various frequencies
 934 from unvegetated (A and C) and vegetated (B and D) sampling locations. Deployment 1 of summer 2022
 935 is shown in (A) and (B) with current-dominated conditions and Deployment 2 is shown in (C) and (D)
 936 with wave-dominated conditions. The $-5/3$ slope lines shown in each graph in A and B indicates the
 937 inertial subrange of turbulence, while in (C) and (D) the addition of wave energy within the wave
 938 frequencies ($0.3 \text{ Hz} < f < 2 \text{ Hz}$) disrupts the characteristic $-5/3$ inertial subrange.

939

940

941

942

943

944

945

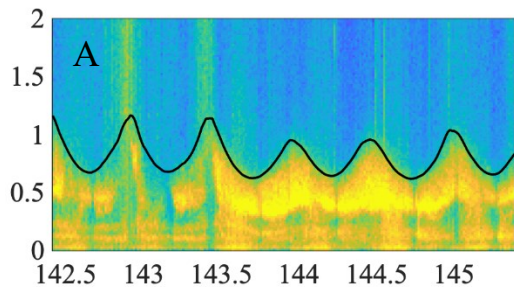
946

947

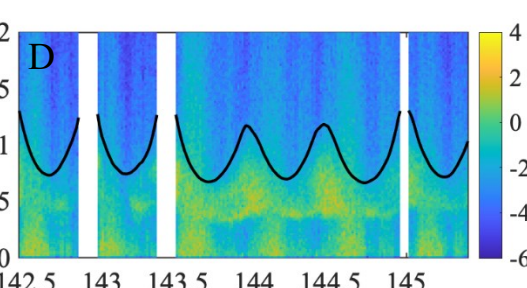
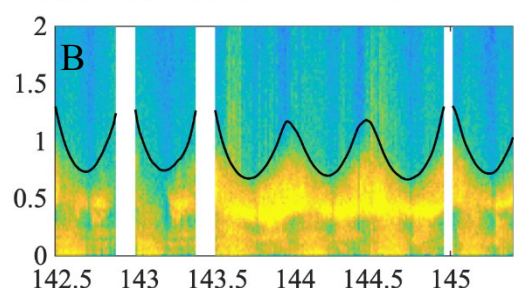
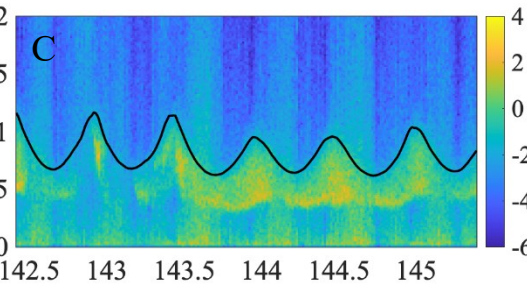
948

949

Horizontal Velocities



Vertical Velocities



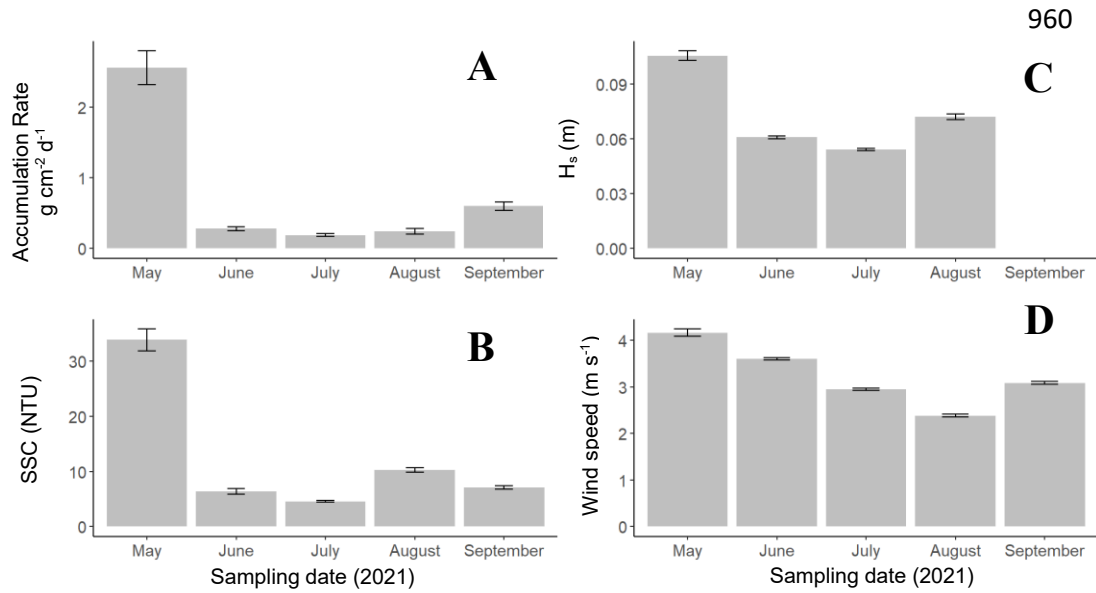
Day of the year (2022)

950 **Figure 8.** Power Spectral Diagram (PSD) of horizontal (A and B) and vertical (C and D) velocities at
 951 frequencies under 2 Hz at unvegetated (A and C) and vegetated (B and D) sampling locations during
 952 Vector deployment 2 at Site 2. Black lines show the lower threshold of expected wave attenuation, which
 953 is inversely related to the square root of the water depth. Gaps in the figure represent periods of no data
 954 collection due to instrument exposure at low tide.

955

956

957
958
959



974
975
976 **Figure 9.** Monthly averages ± 1 SE of (A) sediment accumulation rate, (B) Suspended sediment
977 concentration (C) significant wave height (H_s), and (D) wind speed from Site 1 during 2021.
978

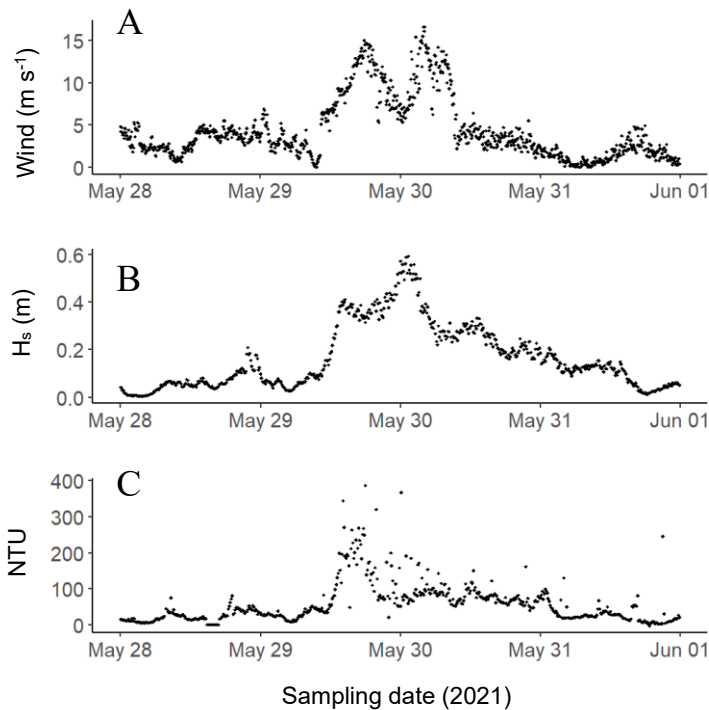
960

979

980

981

982



983

984

985

986

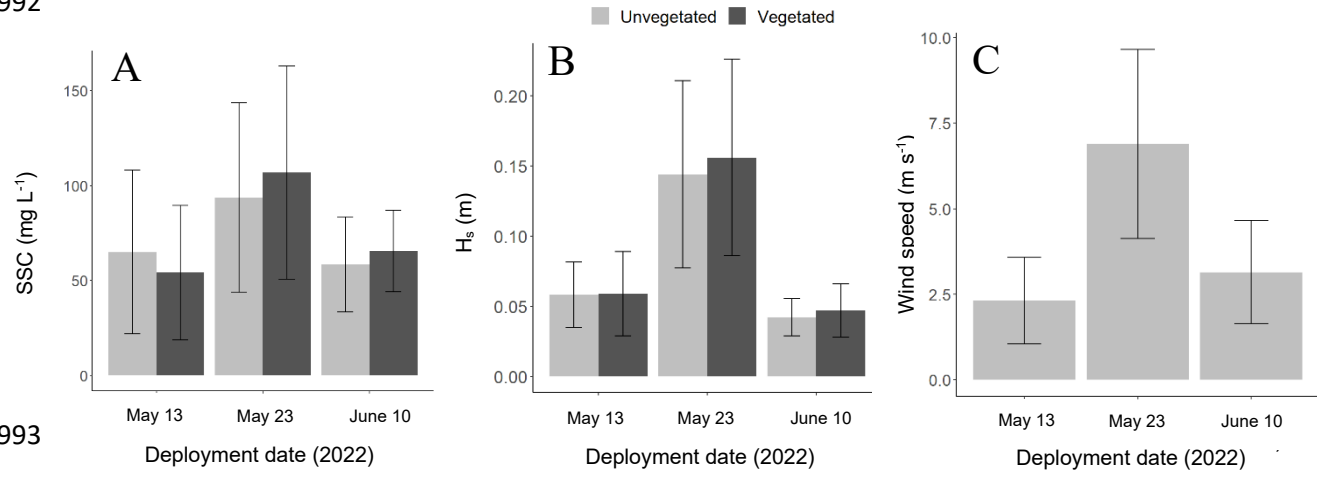
987

988

Sampling date (2021)

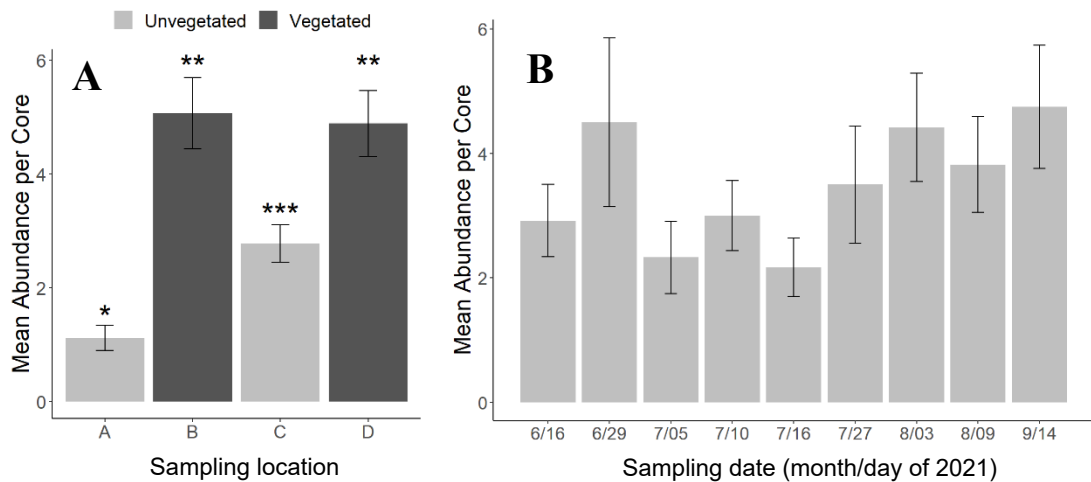
Figure 10: Time series data of (A) wind speed (m/s), (B) significant wave height, H_s (m), and (C) NTU from the vegetated sampling location at Site 1 during a storm from May 28 – June 1, 2021.

989
990
991
992



993
994
995
996
997

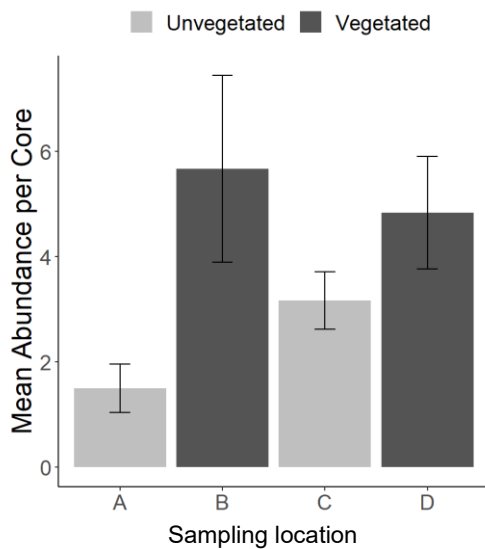
Figure 11. Averages ± 1 SD of A) suspended sediment concentration, B) significant wave height, H_s, and C) wind speed from periods of Vector deployment at Site 2 during summer 2022.



1011
1012
1013 **Figure 12.** A) Mean abundances \pm 1 SE of bivalves per core (core volume= 1390 cm³) from each
1014 sampling location (A-D) averaged over the entire study period of 2021. Location A in naturally bare
1015 seafloor, C in the artificial bare patch, B and D in vegetation 5 and 25 m past the meadow's natural edge,
1016 respectively. Significance denoted with asterisks (one-way ANOVA, $p < 0.001$). B) Mean abundances \pm 1
1017 SE of bivalves per core at all sampling locations from each round of collection (month/day) during
1018 summer 2021. A square-root transformation was applied to abundance values to meet assumptions of
1019 normality.
1020

1021

1022



1023

1024

1025

1026 **Figure 13.** Mean abundances \pm 1 SE of bivalves per core (core volume= 1390 cm^3) from each sampling
1027 location (A-D) averaged over the entire study period of 2022 at site 1. Location A in naturally bare
1028 seafloor, C in the artificial bare patch, B and D in vegetation 5 and 25 m past the meadow's natural edge,
1029 respectively.

1030

1031

1032